PAPER

Check for updates

Automatic identification of chemical moieties†

Jonas Lederer, [ID] *[ab] Michael Gastegger,[ab] Kristof T. Schütt,[ab]
Michael Kampffmeyer, [ID] [c] Klaus-Robert Müller[abdef] and Oliver T. Unke [ID] *[abd]

In recent years, the prediction of quantum mechanical observables with machine learning methods has become increasingly popular. Message-passing neural networks (MPNNs) solve this task by constructing atomic representations, from which the properties of interest are predicted. Here, we introduce a method to automatically identify chemical moieties (molecular building blocks) from such representations, enabling a variety of applications beyond property prediction, which otherwise rely on expert knowledge. The required representation can either be provided by a pretrained MPNN, or be learned from scratch using only structural information. Beyond the data-driven design of molecular fingerprints, the versatility of our approach is demonstrated by enabling the selection of representative entries in chemical databases, the automatic construction of coarse-grained force fields, as well as the identification of reaction coordinates.

1 Introduction

The computational study of structural and electronic properties of molecules is key to many discoveries in physics, chemistry, biology, and materials science. In this context, machine learning (ML) methods have become increasingly popular as a means to circumvent costly quantum mechanical calculations.[1–37] One class of such ML methods are message passing neural networks (MPNNs),[38] which provide molecular property predictions based on end-to-end learned representations of atomic environments.

In contrast to such fine-grained representations, chemists typically characterize molecules by larger substructures (*e.g.* functional groups) to reason about their properties.[39–41] This gives rise to the idea of using MPNNs for the automatic identification of "chemical moieties", or characteristic parts of the molecule, to which its properties can be traced back. Since manually searching for moieties that explain (or are characteristic of) certain properties of molecules is a complex and tedious task, the capability of ML to find patterns and

correlations in data could ease the identification of meaningful substructures drastically.

Previous work has introduced a variety of different approaches to identify substructures in molecules and materials, with objectives ranging from substructure mining[42–47] over molecule generation[48–52] and interpretability of machine learning architectures[53–62] and coarse-graining[63–65] to insights into atomistic simulations.[66] While these methods offer substantial advantages for their specific tasks, it is important to note that most of them are tailored to address singular objectives, thereby limiting their overall applicability. In this work, the primary goal is to introduce a method that prioritizes versatility and generality, aiming to encompass a broader range of potential applications. Hence, to ensure the identification of meaningful moieties that can be utilized for a wide range of applications, a procedure is required (i) to be transferable w.r.t. molecule size, (ii) to provide a substructure decomposition of each molecule which preserves its respective global structure (required for, *e.g.*, coarse-graining), and (iii) to allow for identifying several moieties of the same type in individual molecules (due to a common substructure often appearing multiple times). None of the methods mentioned above meets all of these criteria.

In this work, we propose MoINN (Moiety Identification Neural Network) – a method for the automatic identification of chemical moieties from the representations learned by MPNNs. This is achieved by constructing a soft assignment (or affinity) matrix from the atomic features, which maps individual atoms to different types of multi-atom substructures (Fig. 1, top). By employing representations from MPNNs pretrained on molecular properties, the identified moieties are automatically adapted to the chemical characteristics of interest. Alternatively, it is possible

[a] Berlin Institute of Technology (TU Berlin), 10587 Berlin, Germany.
  E-mail: jonas.lederer@tu-berlin.de, oliver.unke@googlemail.com
[b] BIFOLD - Berlin Institute for the Foundations of Learning and Data, Germany
[c] Department of Physics and Technology, UiT The Arctic University of Norway,
 9019 Tromsø, Norway
[d] Google Deepmind, Germany
[e] Department of Artificial Intelligence, Korea University, Seoul 136-713, Korea
[f] Max Planck Institut für Informatik, 66123 Saarbrücken, Germany
† Electronic supplementary information (ESI) available: Additional details regarding the concept of MoINN, training procedure, applications, and comparison to other graph-pooling approaches. See DOI: https://doi.org/10.1039/d3cp03845a
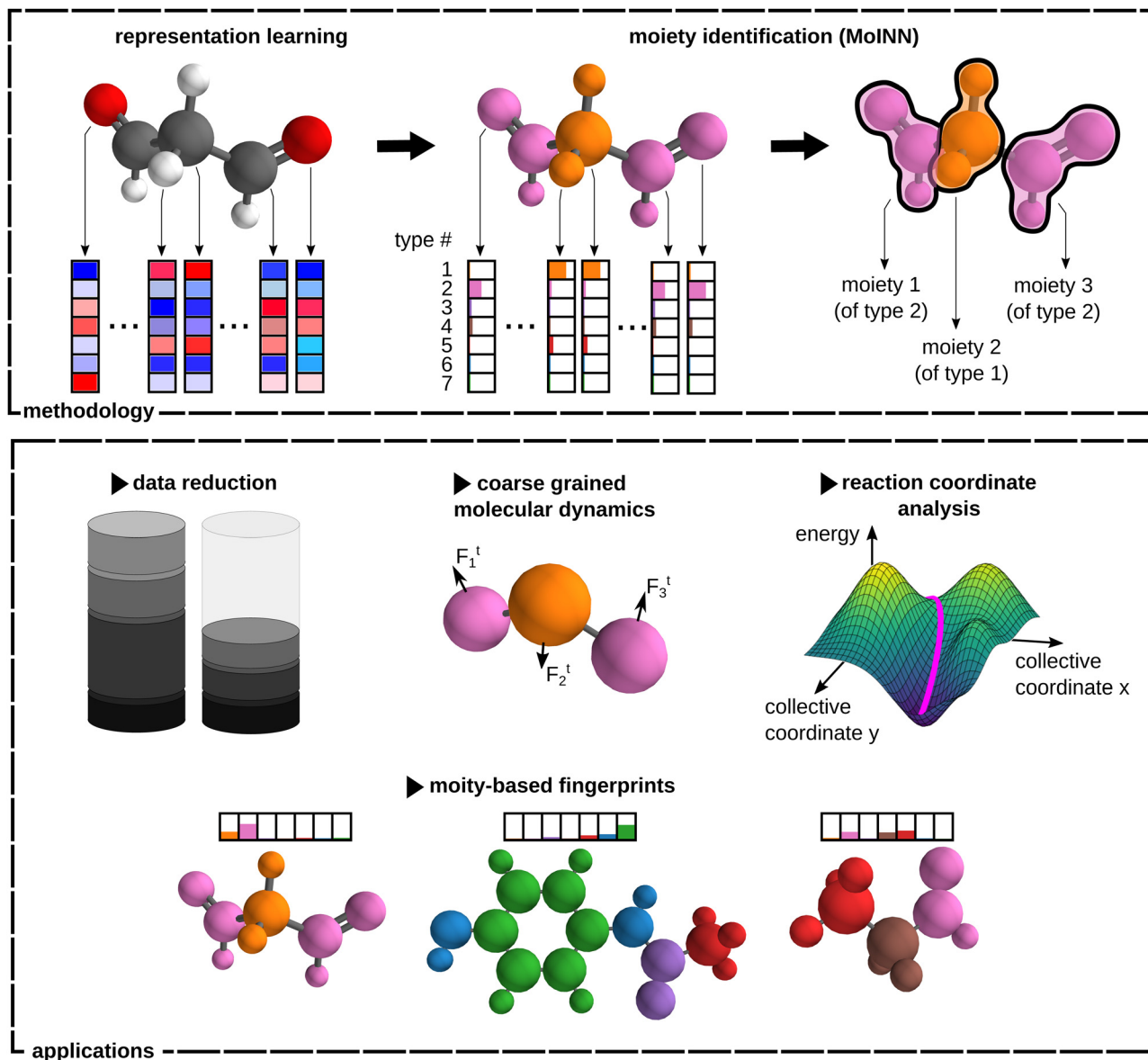
Fig. 1 MoINN methodology and applications. The top shows the moiety identification process for malondialdehyde. First, atomic feature representations (red and blue bars) are learned. Next, MoINN constructs type assignment vectors (pink and orange bars) based on these features. Each entry represents the probability of an atom to be assigned to a specific type of moiety (atoms are colored according to the highest atom-to-type affinity). Based on these assignments and the proximity of atoms, MoINN divides molecules into individual moieties. In this example, three chemical moieties of two distinct types associated with methylene (type 1, orange) and aldehyde (type 2, pink) groups are identified. The moiety representation allows for a variety of applications, which are shown on the bottom. They range from moiety-based fingerprint design, reaction coordinate analysis, and data reduction to coarse grained molecular dynamics.

to find chemically meaningful substructures by training MPNNs coupled with MoINN in an end-to-end manner. Here, only structural information is required and *ab initio* calculations can be avoided. Crucially, MoINN is transferable between molecules of different sizes and automatically determines the appropriate number of moiety types. Multiple occurrences of the same structural motif within a molecule are recognized as the same type of moiety.

We demonstrate the versatility of MoINN by utilizing the identified chemical moieties to solve a range of tasks, which would otherwise require expert knowledge (Fig. 1, bottom). For example, the learned moiety types can serve as molecular fingerprints, which allow to extract the most representative

entries from quantum chemical databases. Beyond that, moieties can be employed as coarse-grained representations of chemical structures, allowing to automatically determine *beads* for the construction of coarse-grained force fields. Finally, we use MoINN to identify reaction coordinates in molecular trajectories based on the transformation of detected moieties.

2 Method

The automated identification of moieties with MoINN corresponds to a clustering of the molecule into different types of

This journal is © the Owner Societies 2023

Phys. Chem. Chem. Phys., 2023, **25**, 26370–26379 | **26371**

PCCP

Paper

chemical environments. Hence, atoms in comparable environments, *i.e.* with similar feature representations (see Section 2.1), are likely to be assigned to the same cluster. In the following, the term "environment types" or short "types" will be used, since each cluster is associated with a specific substructure that exhibits particular chemical characteristics. Note that atoms belonging to the same environment type are not necessarily spatially close, because similar substructures may appear multiple times at distant locations in a molecule. This is why, after atoms have been assigned to environment types (see Section 2.2), individual (spatially disconnected) chemical moieties can be found by introducing an additional distance criterion (see Section 2.3). Both steps are combined to arrive at an unsupervised learning objective for decomposing molecules into chemical moieties (see Section 2.4).

2.1 Representation learning in message passing neural networks

Message passing neural networks (MPNNs)[38] are able to learn atomic feature representations from data in an end-to-end manner (without relying on handcrafted features). They achieve state-of-the-art performance for molecular property prediction, solely taking atomic numbers and atom positions as inputs.[7,11,12,14–17] The representation learning scheme of an MPNN can be described as follows. First, atomic features are initialized to embeddings based on their respective atomic numbers (all atoms of the same element start with the same representation). Subsequently, the features of each atom are iteratively updated by exchanging "messages" with neighboring atoms, which depend on their current feature representations and distances. After several iterations, the features encode the relevant information about the chemical environment of each atom. In this work, we use SchNet[7,9,28] to construct atomic feature representations. In general, however, MoINN is applicable to any other representation learning scheme.

2.2 Assigning atoms to environment types

Starting from F-dimensional atomic feature representations $\mathbf{x}_1,\ldots,\mathbf{x}_N$ of N atoms (*e.g.* obtained from an MPNN), a type assignment matrix $\mathbf{S}$, which maps individual atoms to different environment types, is constructed. Following a similar scheme as Bianchi *et al.*,[67] the type assignment matrix is given by

$$\mathbf{S} = \mathrm{softmax}(\mathrm{SiLU}(\mathbf{X}\mathbf{W}_1)\mathbf{W}_2),\qquad(1)$$

where $\mathbf{W}_1 \in \mathbb{R}^{F\times K}$ and $\mathbf{W}_2 \in \mathbb{R}^{K\times K}$ are trainable weight matrices, the n-th row of the feature matrix $\mathbf{X} \in \mathbb{R}^{N\times F}$ is the representation $\mathbf{x}_n \in \mathbb{R}^F$ of atom n, and SiLU is the Sigmoid Linear Unit activation function.[68] Here, K is a hyperparameter that denotes the maximum number of possible types. As will be shown later, a meaningful number of types is automatically determined from data and largely independent of the choice of K (see Section 2.4). The softmax function ensures that entries $\mathbf{S}_{nk}$ of the $N \times K$ matrix $\mathbf{S}$ obey $\sum_k \mathbf{S}_{nk} = 1 \forall n$ with $\mathbf{S}_{nk} > 0$. Thus, each row of $\mathbf{S}$ represents a probability distribution over the K environment types, with each entry $\mathbf{S}_{nk}$ expressing how likely

atom n should be assigned to type k. Even though assignments are "soft", *i.e.* every atom is partially assigned to multiple environment types, the softmax function makes it unlikely that more than one entry in each row is dominant (closest to 1). The advantage of a soft type assignment matrix is that its computation is well suited for gradient-based optimization. In other contexts, however, it might be more natural to assign atoms unambiguously to only one environment type. For this reason, we also define a "hard" type assignment matrix $\mathbf{S}_{\mathrm{h}} \in \mathbb{R}^{N\times K}$ with entries

$$\mathbf{S}_{\mathrm{h},nk} = \begin{cases} 1 & \mathbf{S}_{nk} > \mathbf{S}_{nj} \forall j \in [0,K)\setminus\{k\} \\ 0 & \mathrm{otherwise} \end{cases},\qquad(2)$$

such that each row contains exactly one non-zero entry equal to 1.

The atomic feature representations making up the matrix $\mathbf{X}$ can either be provided by a pretrained model, or learned in an end-to-end fashion. Depending on the use case, both approaches offer their respective advantages: since the type assignment matrix $\mathbf{S}$ is directly connected to $\mathbf{X}$ *via* eqn (1), pretrained features allow to find types adapted to a specific property of interest. End-to-end learned representations have the advantage that they do not rely on any reference data obtained from computationally demanding quantum mechanical calculations. Instead, they are found from structural information by optimizing an unsupervised learning problem (see Section 2.4).

2.3 Assigning atoms to individual moieties

Molecules may consist of multiple similar or even identical substructures. Consequently, distant atoms with comparable local environments can be assigned to the same type, even though they do not necessarily belong to the same moiety (see Fig. 1). To find the actual chemical moieties, *i.e.* groups of nearby atoms making up a structural motif, we introduce the $N \times N$ moiety similarity matrix given by

$$\mathbf{C} = \mathbf{S}\mathbf{S}^T \circ \mathbf{A},\qquad(3)$$

where "$\circ$" denotes the Hadamard (element-wise) product. Here, the $N \times N$ matrix $\mathbf{S}\mathbf{S}^T$ measures the similarity of the type assignments between atoms, *i.e.* its entries are close to 1 when a pair of atoms is assigned to the same environment type and close to 0 otherwise. The adjacency matrix $\mathbf{A} \in [0,1]^{N\times N}$ on the other hand captures the proximity of atoms. Its entries are defined as

$$\mathbf{A}_{ij}(r_{ij}) = \begin{cases} 0.5\left(1 + \cos\left(\dfrac{\pi r_{ij}}{r_{\mathrm{cut}}}\right)\right) & r_{ij} < r_{\mathrm{cut}} \\ 0 & r_{ij} \geq r_{\mathrm{cut}} \end{cases},\qquad(4)$$

where r_{ij} is the pairwise distance between atoms i and j and r_{cut} is a cutoff distance. For simplicity, we employ a cosine cutoff to assign proximity scores, but more sophisticated schemes are possible (*e.g.* based on the covalent radii of atoms). The combination of $\mathbf{S}\mathbf{S}^T$ and $\mathbf{A}$ ensures that the entries of the similarity matrix $\mathbf{C}$ are close to 1 only if two atoms are both

26372 | *Phys. Chem. Chem. Phys.*, 2023, **25**, 26370–26379

This journal is © the Owner Societies 2023

assigned to the same type and spatially close, in which case they belong to the same chemical moiety.

Analogous to the hard assignment matrix $\mathbf{S}_h$ (see eqn (2)), a hard moiety similarity matrix $\mathbf{C}_h$, which unambiguously assigns atoms to a specific moiety, might be preferable over eqn (3) in some contexts. To this end, we define the matrix

$$\mathbf{C}_h^0 = \mathbf{S}_h \mathbf{S}_h^T \circ \mathbf{A}_{cov}. \tag{5}$$

where $\mathbf{A}_{cov}$ has entries of 1 for each atom-pair connected by a covalent bond (see Section S1, ESI†) and 0 otherwise. $\mathbf{C}_h^0$ describes a graph on which breadth-first search[69] is performed to find its connected components (moieties). This yields a hard similarity matrix $\mathbf{C}_h$, which maps atoms unambiguously to their individual moieties (for further details, please refer to Section S2, ESI†).

2.4 Optimization of environment type assignments and moiety assignments

Chemical moieties are identified by minimizing the unsupervised loss function

$$\mathcal{L} = \mathcal{L}_{cut} + \mathcal{L}_{ortho} + \alpha \mathcal{L}_{ent} , \tag{6}$$

where $\mathcal{L}_{cut}$, $\mathcal{L}_{ortho}$, and $\mathcal{L}_{ent}$ are cut loss, orthogonality loss, and entropy loss, and α is a trade-off hyperparameter. The cut loss $\mathcal{L}_{cut}$[67] penalizes "cutting" the molecule, i.e. assigning spatially close atoms to different moieties. It is defined as

$$\mathcal{L}_{cut} = -\frac{\mathrm{Tr}\left(\mathbf{C}^T \tilde{\mathbf{A}} \mathbf{C}\right)}{\mathrm{Tr}\left(\mathbf{C}^T \tilde{\mathbf{D}} \mathbf{C}\right)} ,$$

where $\tilde{\mathbf{A}} = \mathbf{D}^{-1/2} \mathbf{A} \mathbf{D}^{-1/2} \in \mathbb{R}^{N \times N}$ is a symmetrically normalized adjacency matrix (see eqn (4)). The degree matrix $\mathbf{D} \in \mathbb{R}^{N \times N}$ is diagonal with elements $D_{ii} = \sum_j^N A_{ij}$, where A_{ij} are the entries of $\mathbf{A}$. Consequently, $\tilde{\mathbf{D}}$ is the degree matrix obtained from the entries of $\tilde{\mathbf{A}}$.

To avoid converging to the trivial minimum of $\mathcal{L}_{cut}$ where all atoms are assigned to the same moiety and type, the orthogonality loss[67]

$$\mathcal{L}_{ortho} = \left\| \frac{\mathbf{S} \mathbf{S}^T}{\|\mathbf{S} \mathbf{S}^T\|_F} - \frac{\mathbf{I}_N}{\sqrt{N}} \right\|_F$$

drives the type assignment vectors of different atoms (i.e., the rows of $\mathbf{S}$) to be (close to) orthogonal. Here, $\mathbf{I}_N$ is the $N \times N$ identity matrix and $\|\cdot\|_F$ is the Frobenius norm.

Finally, the entropy term[70]

$$\mathcal{L}_{ent} = -\frac{1}{N} \sum_{nk} S_{nk} \ln(S_{nk})$$

favors "hard" assignments and indirectly limits the number of used types (here, S_{nk}) are the entries of $\mathbf{S}$, see eqn (1)). Without this term, there is no incentive to use fewer than K types, i.e., the model would eventually converge to use as many different types as possible. Hence, by introducing the entropy term, we avoid relying on expert knowledge for choosing K and instead facilitate learning a meaningful number of types from data.

In principle, the number of used types still depends on K and the entropy trade-off factor α. However, as is shown in Section S3 (ESI†), there is a regime of α where the number of used types is largely independent of K (as long as K is sufficiently large). Hence, we arbitrarily choose $K = 100$ in our experiments if not specified otherwise. In Section S4 (ESI†), we demonstrate the influence of different cutoff radii on the model output. The experiments show that for a cutoff radius r_{min} between one and two covalent bond lengths the number of environment types is largely independent of r_{min}.

3 Applications

This section describes several applications of MoINN. First, we use MoINN to identify common moieties in molecular data (Section 3.1). Leveraging these insights, we select representative examples from a database of structures to efficiently reduce the number of reference calculations required for property prediction tasks (Section 3.2). Next, an automated pipeline for coarse-grained molecular dynamics simulations built on top of MoINN is described (Section 3.3). Finally, we demonstrate how to utilize MoINN for automatically detecting reaction coordinates in molecular dynamics trajectories (Section 3.4).

3.1 Identification of chemical moieties

To demonstrate the automatic identification of chemical moieties, we apply MoINN to the QM9 dataset.[71] Here, two different models are considered: one utilizes fixed feature representations provided by a SchNet model pretrained to predict energies, while the other model is trained in an end-to-end fashion on purely structural information. In the following, these will be referred to as the pretrained model and the end-to-end model, respectively. Details on the training of SchNet and MoINN, as well as, a comparison between pretrained model and end-to-end model can be found in Section S4 (ESI†). Also the impact of varying training data size on MoINN outputs is shown there.

Fig. 2 depicts the results for the pretrained MoINN model evaluated on a test set of 1000 molecules that were excluded from the training procedure. The top shows four exemplary molecules with corresponding type assignments and moieties. As expected, we observe that moieties of the same type may occur across different molecules, as well as multiple times in a single molecule. The evaluation of environment types and corresponding moieties for all 1000 molecules (see bottom of Fig. 2) shows that each type is associated with a small set of similar moieties, i.e., the environment types form a "basis" of common substructures that can be combined to form all molecules contained in the dataset. In Section S5.1 (ESI†), we evaluate MoINN w. r. t. various ring systems and the largest identified moieties. We observe that while saturated rings are predominantly divided into several small moieties, MoINN tends to identify aromatic rings as individual entities.

This journal is © the Owner Societies 2023

Phys. Chem. Chem. Phys., 2023, **25**, 26370–26379 | **26373**
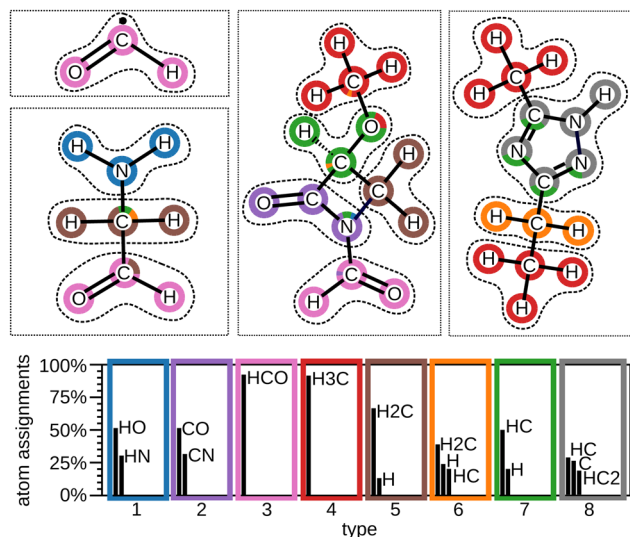
Fig. 2 Common moieties of the QM9 dataset. The top shows four exemplary molecules along with type assignments (colored circles) and moieties (enclosed by dashed lines). The bottom shows the distribution of environment types and corresponding most common moieties for the test set (1000 molecules), black bars indicate the relative amount of atoms assigned to the respective moieties. For each environment type, over 70% of its atom assignments correspond to at most three different moieties.

3.2 Sampling of representative molecules

The quality of the reference dataset used to train ML models greatly impacts their generalization performance.[72] Since the calculation of molecular properties at high levels of theory is computationally demanding, it is desirable to find ways to reduce the amount of reference data needed for training accurate machine learning models. One way to allow for more data efficient training is by sampling a representative subset of data points from chemical space (instead of choosing points randomly). Amongst other benefits, Huang *et al.* have shown that this can be achieved by utilizing small molecular building blocks (atom-in-molecule-based fragments) in the training data.[35] Cersonsky *et al.* have evaluated supervised and unsupervised approaches based on low-rank approximation of the feature matrix and farthest point sampling (FPS).[73] Browning *et al.* utilize a genetic algorithm to find an optimized training set,[74] and Podryabinkin *et al.* proposed an approach based on the D-optimality criterion.[75,76]

In contrast, we aim to find a representative set of molecules that can be understood as a "basis" of molecules that allows to reconstruct the features (fingerprints) of all the remaining molecules as closely as possible. To this end, we define type-based fingerprints from the assignments learned by the end-to-end MoINN model as

$$\mathbf{h}_{\text{MoINN}} = \sum_n S_{nk}(\mathbf{X}) , \qquad (7)$$

where $\mathbf{X}$ denotes the atomic feature matrix and S_{nk} is the assignment matrix entry for the n-th atom and the k-th type. Note that the feature size of the type-based fingerprints is given by the number of environment types $K = 100$. However, due to

the sparsity of the environment types, the effective number of features is 17 (see also Section S4, ESI†).

By stacking the fingerprints $\mathbf{h}_{\text{MoINN}}$ of D molecules on top of each other we obtain the fingerprint matrix $\mathbf{H}_{\text{MoINN}} \in \mathbb{R}^{D \times K}$. To find a possible small subset of molecules ("basis"), which still represents the QM9 dataset sufficiently well, we minimize the loss function

$$\mathcal{L}_{\text{data}} = \|\mathbf{W}\mathbf{H}_{\text{MoINN}} - \mathbf{H}_{\text{MoINN}}\|_F + \lambda \sum_j \sqrt{\sum_i w_{ij}{}^2} , \qquad (8)$$

where $\mathbf{W} \in \mathbb{R}^{D \times D}$ is a trainable weight matrix with entries $\{w_{ij}\}$. The first term in eqn (8) describes the reconstruction error. To avoid converging to the trivial solution, where the trainable matrix $\mathbf{W}$ is simply the identity matrix, we introduce a regularization term that enforces sparse rows in the weight matrix $\mathbf{W}$. The trade-off between both terms can be tuned by the factor λ, *i.e.* larger values of λ will select a smaller subset of representative molecules. Intuitively, minimizing eqn (8) corresponds to selecting a small number of molecules as "basis vectors", from which all other molecules can be (approximately) reconstructed by linear combination.

Based on this procedure, we select several QM9 subsets of different size as training sets and compare them to randomly sampled subsets, and subsets obtained by stratified sampling w. r. t. the number of atoms in each molecule. For each of these subsets, we train five SchNet models and evaluate their average performance (Fig. 3). Models trained on subsets chosen by MoINN perform significantly better than those trained on randomly sampled subsets and stratified sampled subsets. This effect is most pronounced for small training set sizes. Thus, selecting data with MoINN is most useful in a setting where only few data points can be afforded, *e.g.* when using a high level of theory to perform reference calculations. For more details on the experiment and a comprehensive discussion of the results please refer to Section S5.2 (ESI†).
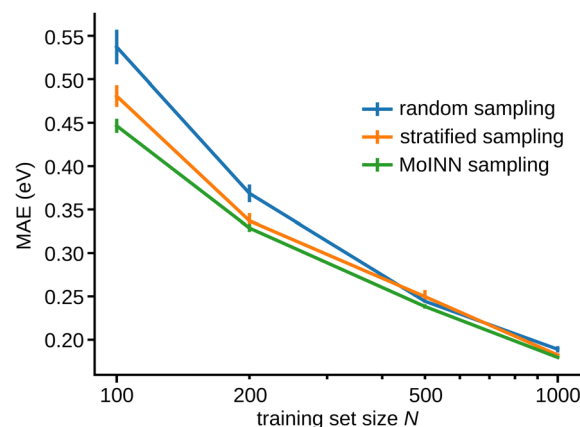

Fig. 3 Mean absolute error (MAE) of energy predictions for SchNet models trained on randomly sampled training sets (blue), training sets obtained by stratified sampling (orange) and training sets selected with MoINN (green). Each data point is averaged over five independent training runs and standard errors are indicated by error bars.

26374 | *Phys. Chem. Chem. Phys.*, 2023, **25**, 26370–26379

This journal is © the Owner Societies 2023

3.3 Coarse-grained molecular dynamics

While ML force fields accelerate *ab initio* MD simulations by multiple orders of magnitude,[13] the study of very large molecular structures is still computationally demanding. Coarse-graining (CG) reduces the dimensionality of the problem by representing groups of atoms as single interaction sites. Most approaches rely on systematically parametrized CG force fields,[77,78] but also data driven approaches have been proposed.[79–83] In both cases, however, the coarse-grained "beads" are usually determined manually by human experts.[84]

Here, we propose an automated pipeline for coarse-grained molecular dynamics simulations (CG-MD), which comprises atomistic SchNet models for noise reduction, MoINN for reducing the molecule's degrees of freedom, and a SchNet model trained on the CG representation for simulating the CG dynamics. We apply this approach to the trajectory of alanine-dipeptide in water,[85,86] which is a commonly used model system for comparing different CG methods.[79–81]

The CG representation, shown in Fig. 4, is inferred from the environment types and moieties provided by the pretrained MoINN model described in Section 3.1, which has been trained on the QM9 dataset. For a comparison to conventional CG representations such as, *e.g.*, OPLS-UA,[87,88] or an automated CG approach[89] for the Martini force field,[77] please refer to section S5.3 (ESI†). The original atomistic trajectory of alanine-dipeptide does not include reference energies. This is because the dynamics have been simulated in solvent, which introduces noise to the energy of the system if the solvent is not modeled explicitly. The data contains forces for all atoms in the alanine-dipeptide molecule, which implicitly include interactions with solvent molecules. However, sparsely sampled transition regions between conformers are challenging to learn with force targets only. Coarse-graining introduces additional noise on the energies and forces[81] since some information about the atom positions is discarded.

To reduce the noise, we train an ensemble of five SchNet models to provide a force field for alanine-dipeptide at atomic resolution. Subsequently, we use the corresponding forces $\hat{\mathbf{F}}$ and energies $\hat{U}$ as targets for training the CG SchNet model in a force-matching scheme adapted from ref. 79–81, 90, 91 (see Section S5.3 for details, ESI†). Based on the CG SchNet model, we run MD simulations in the *NVT* ensemble at room temperature (300 K). The trajectories are initialized according to the
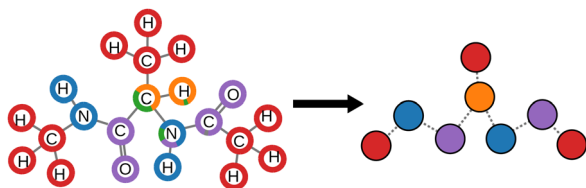

Fig. 4 Automated coarse-graining with MoINN. On the left, the alanine-dipeptide molecule is depicted at atomic resolution, assigned environment types are indicated by colored circles. On the right, the corresponding coarse-grained representation, derived from environment types and moiety assignments, is shown.
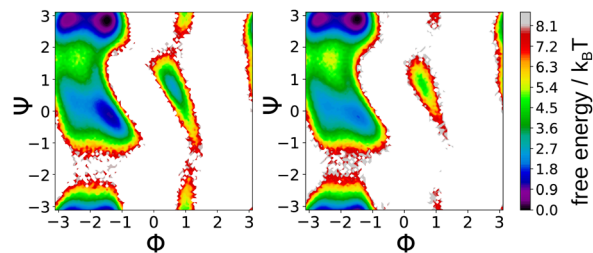

Fig. 5 Ramachandran plots of the free energy surface of alanine-dipeptide with respect to the torsion angles ϕ and ψ for the atomistic MD (left) and the coarse-grained MD (right) (ϕ and ψ are computed with respect to the coarse-grained geometry).

Boltzmann distribution at the six minima of the potential energy surface. For keeping the temperature constant, we use a Langevin thermostat. Fig. 5 shows that the free energy surfaces derived from the all-atom and CG trajectories are in good agreement.

MoINN also allows for coarse-graining structures outside the scope of QM9. This is shown in Fig. 6 for decaalanine. The provided CG representation resembles the commonly used OPLS-UA representation.[87,88] However it is striking that the type of terminal methyl groups differs from that of the backbone methyl groups, while in the OPLS-UA representation, by construction, those groups are considered to be interchangeable. For more details how the CG representation is derived from the provided environment types, see Section S5.3 (ESI†).

3.4 Dynamic clustering and reaction coordinate analysis

MoINN is also capable of learning environment types for molecular trajectories. In this case, the types describe "dynamic clusters", which can be useful, *e.g.*, for determining collective variables that describe chemical reactions. As a demonstration of this concept, we consider two chemical reactions, namely the proton transfer reaction in malondialdehyde and the Claisen rearrangement of allyl *p*-tolyl ether (see ref. 92 and 93 for details on how the trajectories were obtained). We train individual end-to-end MoINN models on each reaction trajectory.

For each time step in the trajectory, we construct a high-dimensional coordinate vector

$$\mathbf{h}_{\mathrm{dyn}} = (S_{11}, S_{12}, \ldots, S_{1K}, S_{21}, \ldots, S_{2K}, \ldots, S_{NK}),$$

which consists of the type assignment matrix entries $\{S_{nk}\}$. By applying standard dimensionality reduction methods like principal component analysis (PCA),[94,95] it is possible to extract a low-dimensional representation of the largest structural changes in the trajectory. For the two considered cases, we find that a one-dimensional reaction coordinate given by the first principal component provides a good description of the dynamic process and shows a prominent "jump" when the reaction happens (see Fig. 7). In Section S5.4 (ESI†), we show that the reaction coordinate derived from MoINN allows for a more clear distinction between reactants and product than simply using the adjacency matrix based on the pairwise distances of atoms.
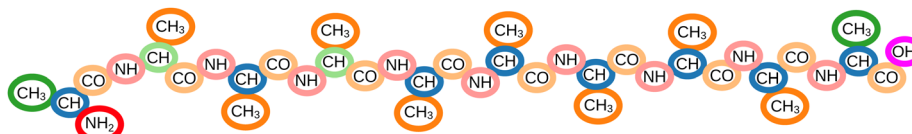
This journal is © the Owner Societies 2023

Phys. Chem. Chem. Phys., 2023, **25**, 26370–26379 | **26375**

Fig. 6 CG-representation of deca-alanine inferred from environment types provided by MoINN.
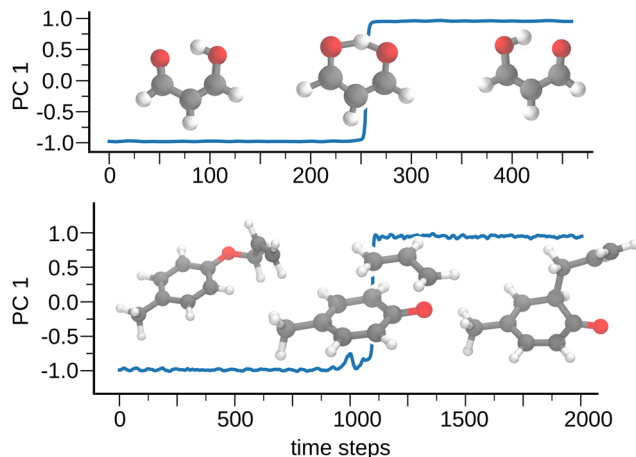
Fig. 7 Automatic detection of reaction coordiantes for the proton transfer in malondialdehyde (top) an the Claisen rearrangement of allyl *p*-tolyl ether (bottom). The identified reaction coordinate is plotted w.r.t. the time step of the respective trajectory.

4 Discussion

Owing to its computational efficiency, interpretability, and transferability, MoINN is applicable to a wide range of different tasks which otherwise rely on expert knowledge. MoINN involves a representation-based pooling approach which shares common ideas with the graph-pooling approaches DiffPool[70] and MinCut.[67] Latter describe the acquisition of a soft assignment matrix, which allows to pool graph nodes (atoms) to representative super-nodes (atom groups). In DiffPool the assignment matrix is learned utilizing GNNs, while MinCut employs a multilayer perceptron (MLP) architecture. Both methods introduce unsupervised loss functions to ensure a reasonable number of super-nodes while preferably grouping nearby nodes. Similar to MinCut, MoINN learns a mapping from atomic feature representations to type assignments by two dense layers (an MLP). The shallow network architecture results in computationally cheap training and inference. As the most prominent difference, MoINN distinguishes between individual moieties and environment types, while DiffPool and MinCut handle those entities interchangeably. As a result, MoINN stands out with regards to interpretability and transferability.

The distinction between moieties and environment types allows for a more detailed analysis of the identified substructures. While the environment types explain the composition and conformation of the molecular substructures, the moieties represent individual molecular building blocks. Besides the benefits with regards to interpretability, the distinction

between moieties and environment types allows to identify multiple identical moieties in the same molecule. This feature is particularly useful for molecular systems since those often possess atom groups (moieties) of the same type multiple times. In contrast, pooling distant nodes is penalized when utilizing MinCut or DiffPool. Hence, even though some distant nodes might exhibit similar feature representations, they are unlikely to be grouped together. This makes it difficult to find common moieties and might hamper transferability w.r.t. molecules of different size, since the mapping between atoms and atom groups becomes more sensitive to small changes in the feature representations. For more details on this problem, please refer to Section S6 (ESI†).

Another approach that allows for identifying reoccurring patterns in molecular data was proposed by Gasparotto *et al.* called PAMM.[66] This method utilizes Gaussian mixture models to recognize reoccurring patterns in atomistic simulation data, and has shown to be of great use regarding the identification of hydrogen bonds. While MoINN and PAMM share the scheme of identifying motifs in molecular data, the underlying concepts are very different. One point that makes MoINN unique is its end-to-end framework. In contrast to PAMM, MoINN can be integrated into different neural network architectures and optimization tasks. This feature, *inter alia*, allows to obtain insight into the representation learning of neural networks. Furthermore, while the number of clusters needs to be specified for the Gaussian mixture model, MoINN does not require prior knowledge regarding the number of environment types but learns them. This makes MoINN well transferable (the transferability of MoINN regarding the molecule size is shown in Section S5.3, ESI†).

5 Conclusion and outlook

We have introduced MoINN, a versatile approach capable of automatically identifying chemical moieties in molecular data from the representations learned by MPNNs. Our method gives insight into the representation learning of MPNNs by identifying environment types based on the learned feature environments of the underlying MPNN. MoINN is differentiable, and thus, it can be exploited for a variety of applications beyond those showcased in this work. Depending on the task at hand, MoINN can be trained based on pretrained representations or in an end-to-end fashion. While pretrained representations may lead to moieties that are associated with a certain molecular property, training MoINN in an end-to-end fashion circumvents costly first principle calculations. By construction, MoINN allows to identify multiple moieties of the same type

26376 | *Phys. Chem. Chem. Phys.*, 2023, **25**, 26370–26379

This journal is © the Owner Societies 2023

(*e.g.* corresponding to the same functional group) in individual molecules. This design choice also makes MoINN transferable w.r.t. molecule size and allows to automatically determine a reasonable number of moieties and environment types without relying on expert knowledge. The soft assignment of atoms to the respective environment types ensures a transparent identification of distinct moieties (compare Section S5.3, ESI†).

Representing molecules as a composition of chemical moieties paves the way for various applications, some of which have been demonstrated in this work: human-readable and interpretable fingerprints can be directly extracted from the environment types identified by MoINN and they can be employed for selecting representative molecules from quantum mechanical databases to reduce the number of *ab initio* reference data necessary for training accurate models. Further, we have proposed a CG-MD simulation pipeline based on MoINN, which includes all necessary steps from the identification of CG representations, the machine learning of a CG force field, up to the MD simulation of the CG molecule. The pipeline is fully automatic and does not require expert knowledge. As another example, we have presented the dynamic clustering of chemical reactions, demonstrating that the environment types identified by MoINN capture conformational information that can be used to define reaction coordinates.

A promising avenue for future work is the application of MoINN in the domain of generative models.[25,26] Jin *et al.* have shown that generating molecules in a hierarchical fashion can be advantageous.[48,50] MoINN could help to identify promising motifs for molecule generation and hence facilitate the discovery of large molecules. Furthermore, MoINN could be utilized to analyze other interesting reactions. In summary, MoINN extends the applicability of MPNNs to a wide range of chemical problems otherwise relying on expert knowledge. In addition, we expect applications of MoINN to allow new insights into large-scale chemical phenomena, where MPNNs acting on individual atoms are prohibitively computationally expensive to evaluate.

Software and data availability

We provide the source code of MoINN on GitHub **https://github.com/jnsLs/MoINN**. For the experiments we solely utilized public datasets, which can be found at **https://www.quantum-machine.org/**.

Author contributions

Jonas Lederer, Oliver T. Unke, Michael Gastegger, and Kristof T. Schütt conceived the work. Together with Michael Kampffmeyer they developed the method. Jonas Lederer, Oliver T. Unke, Michael Gastegger, Kristof T. Schütt and Klaus-Robert Müller collected promising application ideas. Jonas Lederer implemented the method and performed the experiments. All the authors contributed to the discussion, writing, editing, and revision of the manuscript.

Conflicts of interest

The authors have no conflicts of interest to declare.

Acknowledgements

Notes and references

1 J. Behler and M. Parrinello, *Phys. Rev. Lett.*, 2007, **98**, 146401.
2 A. P. Bartók, M. C. Payne, R. Kondor and G. Csányi, *Phys. Rev. Lett.*, 2010, **104**, 136403.
3 M. Rupp, A. Tkatchenko, K.-R. Müller and O. A. von Lilienfeld, *Phys. Rev. Lett.*, 2012, **108**, 058301.
4 K. Schütt, P.-J. Kindermans, H. E. S. Felix, S. Chmiela, A. Tkatchenko and K.-R. Müller, *Neural Information Processing Systems*, 2017, pp. 991–1001.
5 S. Chmiela, A. Tkatchenko, H. E. Sauceda, I. Poltavsky, K. T. Schütt and K.-R. Müller, *Sci. Adv.*, 2017, **3**, e1603015.
6 L. Zhang, J. Han, H. Wang, R. Car and W. E, *Phys. Rev. Lett.*, 2018, **120**, 143001.
7 K. T. Schütt, H. E. Sauceda, P.-J. Kindermans, A. Tkatchenko and K.-R. Müller, *J. Chem. Phys.*, 2018, **148**, 241722.
8 L. Zhang, J. Han, H. Wang, R. Car and W. E, *Phys. Rev. Lett.*, 2018, **120**, 143001.
9 K. T. Schütt, P. Kessel, M. Gastegger, K. Nicoli, A. Tkatchenko and K. R. Müller, *J. Chem. Theory Comput.*, 2018, **15**, 448–455.
10 H. E. Sauceda, S. Chmiela, I. Poltavsky, K.-R. Müller and A. Tkatchenko, *Machine Learning Meets Quantum Physics*, Springer, 2020, pp. 277–307.
11 O. T. Unke and M. Meuwly, *J. Chem. Theory Comput.*, 2019, **15**, 3678–3693.
12 K. Schütt, O. Unke and M. Gastegger, *Proceedings of the 38th International Conference on Machine Learning*, 2021, pp. 9377–9388.
13 O. T. Unke, S. Chmiela, H. E. Sauceda, M. Gastegger, I. Poltavsky, K. T. Schütt, A. Tkatchenko and K.-R. Müller, *Chem. Rev.*, 2021, **121**, 10142–10186.
14 O. T. Unke, S. Chmiela, M. Gastegger, K. T. Schütt, H. E. Sauceda and K.-R. Müller, *Nat. Commun.*, 2021, **12**, 7273.

This journal is © the Owner Societies 2023

Phys. Chem. Chem. Phys., 2023, **25**, 26370–26379 | **26377**

15 J. Klicpera, J. Groß and S. Günnemann, International Conference on Learning Representations (ICLR), 2020.

16 S. Batzner, A. Musaelian, L. Sun, M. Geiger, J. P. Mailoa, M. Kornbluth, N. Molinari, T. E. Smidt and B. Kozinsky, *Nat. Commun.*, 2022, **13**, 2453.

17 K. T. Schütt, F. Arbabzadah, S. Chmiela, K. R. Müller and A. Tkatchenko, *Nat. Commun.*, 2017, **8**, 13890.

18 F. Noé, A. Tkatchenko, K.-R. Müller and C. Clementi, *Annu. Rev. Phys. Chem.*, 2020, **71**, 361–390.

19 O. A. von Lilienfeld, K.-R. Müller and A. Tkatchenko, *Nat. Rev. Chem.*, 2020, **4**, 347–358.

20 J. A. Keith, V. Vassilev-Galindo, B. Cheng, S. Chmiela, M. Gastegger, K.-R. Müller and A. Tkatchenko, *Chem. Rev.*, 2021, **121**, 9816–9872.

21 K. T. Butler, D. W. Davies, H. Cartwright, O. Isayev and A. Walsh, *Nature*, 2018, **559**, 547–555.

22 S. Chmiela, H. E. Sauceda, K.-R. Müller and A. Tkatchenko, *Nat. Commun.*, 2018, **9**, 3887.

23 J. S. Smith, O. Isayev and A. E. Roitberg, *Chem. Sci.*, 2017, **8**, 3192–3203.

24 M. Popova, O. Isayev and A. Tropsha, *Sci. Adv.*, 2018, **4**, eaap7885.

25 N. W. Gebauer, M. Gastegger and K. T. Schütt, Proceedings of the 33rd International Conference on Neural Information Processing Systems, 2019, pp. 7566-7578.

26 N. W. Gebauer, M. Gastegger, S. S. Hessmann, K.-R. Müller and K. T. Schütt, *Nat. Commun.*, 2022, **13**, 973.

27 S. Chmiela, H. E. Sauceda, I. Poltavsky, K.-R. Müller and A. Tkatchenko, *Comput. Phys. Commun.*, 2019, **240**, 38–45.

28 K. T. Schütt, S. S. P. Hessmann, N. W. A. Gebauer, J. Lederer and M. Gastegger, *J. Chem. Phys.*, 2023, **158**, 144801.

29 S. Chmiela, V. Vassilev-Galindo, O. T. Unke, A. Kabylda, H. E. Sauceda, A. Tkatchenko and K.-R. Müller, *Sci. Adv.*, 2023, **9**, eadf0873.

30 J. Lederer, W. Kaiser, A. Mattoni and A. Gagliardi, *Adv. Theory Simul.*, 2019, **2**, 1800136.

31 A. Musaelian, S. Batzner, A. Johansson, L. Sun, C. J. Owen, M. Kornbluth and B. Kozinsky, *Nat. Commun.*, 2023, **14**, 579.

32 J. Gasteiger, J. Groß and S. Günnemann, International Conference on Learning Representations (ICLR), 2020.

33 J. Gasteiger, S. Giri, J. T. Margraf and S. Günnemann, *Machine Learning for Molecules Workshop*, 2020.

34 S. Doerr, M. Majewski, A. Pérez, A. Kramer, C. Clementi, F. Noe, T. Giorgino and G. De Fabritiis, *J. Chem. Theory Comput.*, 2021, **17**, 2355–2363.

35 B. Huang and O. A. von Lilienfeld, *Nat. Chem.*, 2020, **12**, 945–951.

36 B. Huang and O. A. Von Lilienfeld, *Chem. Rev.*, 2021, **121**, 10001–10036.

37 K. Hansen, F. Biegler, R. Ramakrishnan, W. Pronobis, O. A. Von Lilienfeld, K.-R. Muller and A. Tkatchenko, *J. Phys. Chem. Lett.*, 2015, **6**, 2326–2331.

38 J. Gilmer, S. S. Schoenholz, P. F. Riley, O. Vinyals and G. E. Dahl, Proceedings of the 34th International Conference on Machine Learning-Volume 70, 2017, pp. 1263-1272.

39 B. E. Evans, K. E. Rittle, M. G. Bock, R. M. DiPardo, R. M. Freidinger, W. L. Whitter, G. F. Lundell, D. F. Veber,

P. S. Anderson, R. S. L. Chang, V. J. Lotti, D. J. Cerino, T. B. Chen, P. J. Kling, K. A. Kunkel, J. P. Springer and J. Hirshfield, *J. Med. Chem.*, 1988, **31**, 2235–2246.

40 C. D. Duarte, E. J. Barreiro and C. A. Fraga, *Mini Rev. Med. Chem.*, 2007, **7**, 1108–1119.

41 T. L. Lemke, *Review of organic functional groups: introduction to medicinal organic chemistry*, Lippincott Williams & Wilkins, 2003.

42 P. Ertl, *J. Cheminf.*, 2017, **9**, 1–7.

43 J. Klekota and F. P. Roth, *Bioinformatics*, 2008, **24**, 2518–2525.

44 Y. Yamanishi, E. Pauwels, H. Saigo and V. Stoven, *J. Chem. Inf. Model.*, 2011, **51**, 1183–1194.

45 C. Borgelt and M. R. Berthold, 2002 IEEE International Conference on Data Mining, 2002. Proceedings., 2002, pp. 51-58.

46 M. Coatney and S. Parthasarathy, Third IEEE Symposium on Bioinformatics and Bioengineering, 2003. Proceedings., 2003, pp. 336-340.

47 A. T. Brint and P. Willett, *J. Chem. Inf. Comput. Sci.*, 1987, **27**, 152–158.

48 W. Jin, R. Barzilay and T. Jaakkola, International Conference on Machine Learning, 2020, pp. 4839-4848.

49 T. S. Hy and R. Kondor, *Multiresolution Graph Variational Autoencoder*, 2021.

50 W. Jin, R. Barzilay and T. Jaakkola, *ICML*, 2018.

51 W. Jin, R. Barzilay and T. Jaakkola, International Conference on Machine Learning, 2020, pp. 4849-4859.

52 M. Guarino, A. Shah and P. Rivas, 2017.

53 G. Montavon, W. Samek and K.-R. Müller, *Digital Signal Processing*, 2018, **73**, 1–15.

54 W. Samek, G. Montavon, S. Lapuschkin, C. J. Anders and K.-R. Müller, *Proc. IEEE*, 2021, **109**, 247–278.

55 T. Schnake, O. Eberle, J. Lederer, S. Nakajima, K. T. Schütt, K.-R. Müller and G. Montavon, *IEEE Trans. Pattern Analysis Machine Intelligence*, 2022, **44**, 7581–7596.

56 E. Noutahi, D. Beani, J. Horwood and P. Tossou, arXiv: 1905.11577 [cs, q-bio, stat], 2020.

57 K. McCloskey, A. Taly, F. Monti, M. P. Brenner and L. J. Colwell, *Proc. Natl. Acad. Sci. U. S. A.*, 2019, **116**, 11624–11629.

58 B. Chen, T. Wang, C. Li, H. Dai and L. Song, International Conference on Learning Representations, 2020.

59 A. Mukherjee, A. Su and K. Rajan, *J. Chem. Inf. Model.*, 2021, **61**, 2187–2197.

60 H. E. Webel, T. B. Kimber, S. Radetzki, M. Neuenschwander, M. Nazaré and A. Volkamer, *J. Comput.-Aided Mol. Des.*, 2020, **34**, 731–746.

61 A. H. Khasahmadi, K. Hassani, P. Moradi, L. Lee and Q. Morris, International Conference on Learning Representations, 2019.

62 S. Letzgus, P. Wagner, J. Lederer, W. Samek, K.-R. Müller and G. Montavon, *IEEE Signal Processing Magazine*, 2022, **39**, 40–58.

63 W. Wang and R. Gómez-Bombarelli, *npj Comput. Mater.*, 2019, **5**, 1–9.

64 M. A. Webb, J.-Y. Delannoy and J. J. Pablo, *J. Chem. Theory Comput.*, 2019, **15**, 1199–1208.

26378 | *Phys. Chem. Chem. Phys.*, 2023, **25**, 26370–26379

This journal is © the Owner Societies 2023

65 M. Chakraborty, C. Xu and A. D. White, *J. Chem. Phys.*, 2018, **149**, 134106.

66 P. Gasparotto and M. Ceriotti, *J. Chem. Phys.*, 2014, **141**, 174110.

67 F. M. Bianchi, D. Grattarola and C. Alippi, International conference on machine learning, 2020, pp. 874–883.

68 D. Hendrycks and K. Gimpel, *arXiv*, 2016, preprint, arXiv:1606.08415.

69 S. S. Skiena, *The Algorithm Design Manual*, Springer Publishing Company, Incorporated, 2nd edn, 2008, pp. 162–166.

70 Z. Ying, J. You, C. Morris, X. Ren, W. Hamilton and J. Leskovec, *Neural Information Processing Systems*, 2018, pp. 4800–4810.

71 R. Ramakrishnan, P. O. Dral, M. Rupp and O. A. Von Lilienfeld, *Sci. Data*, 2014, **1**, 1–7.

72 L. I. Vazquez-Salazar, E. Boittier, O. T. Unke and M. Meuwly, *J. Chem. Theory Comput.*, 2021, **17**, 4769–4785.

73 R. K. Cersonsky, B. A. Helfrecht, E. A. Engel, S. Kliavinek and M. Ceriotti, *Machine Learning: Sci. Technol.*, 2021, **2**, 035038.

74 N. J. Browning, R. Ramakrishnan, O. A. Von Lilienfeld and U. Roethlisberger, *J. Phys. Chem. Lett.*, 2017, **8**, 1351–1359.

75 E. V. Podryabinkin and A. V. Shapeev, *Comput. Mater. Sci.*, 2017, **140**, 171–180.

76 B. Settles, 2009.

77 S. J. Marrink, H. J. Risselada, S. Yefimov, D. P. Tieleman and A. H. De Vries, *J. Phys. Chem. B*, 2007, **111**, 7812–7824.

78 E. Brini, E. A. Algaer, P. Ganguly, C. Li, F. Rodríguez-Ropero and N. F. A. van der Vegt, *Soft Matter*, 2013, **9**, 2108–2119.

79 B. E. Husic, N. E. Charron, D. Lemm, J. Wang, A. Pérez, M. Majewski, A. Krämer, Y. Chen, S. Olsson and G. de Fabritiis, *et al.*, *J. Chem. Phys.*, 2020, **153**, 194101.

80 J. Wang, S. Chmiela, K.-R. Müller, F. Noé and C. Clementi, *J. Chem. Phys.*, 2020, **152**, 194106.

81 J. Wang, S. Olsson, C. Wehmeyer, A. Pérez, N. E. Charron, G. De Fabritiis, F. Noé and C. Clementi, *ACS Cent. Sci.*, 2019, **5**, 755–767.

82 L. Zhang, J. Han, H. Wang, R. Car and W. E, *J. Chem. Phys.*, 2018, **149**, 034101.

83 Y. Chen, A. Krämer, N. E. Charron, B. E. Husic, C. Clementi and F. Noé, *J. Chem. Phys.*, 2021, **155**, 084101.

84 S. Riniker, J. R. Allison and W. F. van Gunsteren, *Phys. Chem. Chem. Phys.*, 2012, **14**, 12423–12430.

85 F. Nüske, H. Wu, J.-H. Prinz, C. Wehmeyer, C. Clementi and F. Noé, *J. Chem. Phys.*, 2017, **146**, 094104.

86 C. Wehmeyer and F. Noé, *J. Chem. Phys.*, 2018, **148**, 241703.

87 W. L. Jorgensen and J. Tirado-Rives, *J. Am. Chem. Soc.*, 1988, **110**, 1657–1666.

88 W. L. Jorgensen, D. S. Maxwell and J. Tirado-Rives, *J. Am. Chem. Soc.*, 1996, **118**, 11225–11236.

89 T. D. Potter, E. L. Barrett and M. A. Miller, *J. Chem. Theory Comput.*, 2021, **17**, 5777–5791.

90 W. G. Noid, P. Liu, Y. Wang, J.-W. Chu, G. S. Ayton, S. Izvekov, H. C. Andersen and G. A. Voth, *J. Chem. Phys.*, 2008, **128**, 244115.

91 W. G. Noid, J.-W. Chu, G. S. Ayton, V. Krishna, S. Izvekov, G. A. Voth, A. Das and H. C. Andersen, *J. Chem. Phys.*, 2008, **128**, 244114.

92 K. Schütt, M. Gastegger, A. Tkatchenko, K.-R. Müller and R. J. Maurer, *Nat. Commun.*, 2019, **10**, 5024.

93 M. Gastegger, K. T. Schütt and K.-R. Müller, *Chem. Sci.*, 2021, **12**, 11473–11483.

94 H. Hotelling, *J. Educ. Psy.*, 1933, **24**, 498–520.

95 K. Pearson, *London, Edinburgh Dublin Philos. Mag. J. Sci.*, 1901, **2**, 559–572.

This journal is © the Owner Societies 2023

Phys. Chem. Chem. Phys., 2023, **25**, 26370–26379 | **26379**